Supplementary Materials

Synergy mechanisms of algal extracellular organic matter and manganese oxides in 17α-ethinylestradiol photochemical degradation

Zhicheng Liao [1, 3, 4], Huan He (✉)[1], Feiyuan Liu [1], Jingye Cui [1], Ziwei Guo [1], Al-Anazi Abdulaziz [3], Bin Huang [1], Hongwen Sun [2, 4], Xuejun Pan (✉)[1, 4]

1 Faculty of Environmental Science and Engineering, Kunming University of Science and Technology, Kunming 650500, China

2 Ministry of Education Key Laboratory of Pollution Processes and Environmental Criteria, College of Environmental Science and Engineering, Nankai University, Tianjin 300350, China

3 Department of Chemical Engineering, College of Engineering, King Saud University, Riyadh 11421, Saudi Arabia

4 Southwest United Graduate School, Kunming 650092, China

✉ Corresponding authors

E-mail: huanhe08@kust.edu.cn (H. He); xjpan@kust.edu.cn (X. Pan)

Text S1 Chemicals.

Pyrophosphate (PP, ≥ 95%), 2,4,6-trimethylphenol (TMP, 97%), furfuryl alcohol (FFA, 98%), acetonitrile (≥ 99.9%), EE2 (≥ 98%), manganese(III) acetate dihydrate (97.0%), dimethyl sulfoxide (DMSO, ≥ 99.7%), furfuryl alcohol (FFA, 98.0%), 2,4,6-trimethylphenol (TMP, 97.0%) and trifluoroacetic acid (≥ 99.0%) were obtained from Sigma-Aldrich (USA). The 5,5-dimethyl-1-pyrroline N-oxide (DMPO, ≥ 98.0%) was bought from DOJINDO Laboratories, Japan. Manganese chloride ($MnCl_2$, ≥ 99%), potassium permanganate ($KMnO_4$, 99.5%), potassium hydroxide (KOH, 95%), 4-hydroxy-2,2,6,6-tetramethylpiperidine (TEMP, > 98.0%), oxalate (99.0%) and terephthalic acid (TPA, 99%) were purchased from Aladdin (China). The sulfate, chloride and nitrate standard solutions used came from Guobiao (Beijing) Testing & Certification Co., Ltd., China. The 2-hydroxyterephthalic acid (2-hTPA, > 98.0%) was bought from Tokyo Chemical Industry CO., Japan. Additional chemicals were procured from Xilong Chemicals (China).

Text S2 Determinations of reagents and reactive species.

Determination of EE2

EE2 concentrations were determined using high-performance liquid chromatography (HPLC) equipped with a C18 reversed-phase separation column (4.6 × 150 mm, 5 μm particle size) and a fluorescence detector. The mobile phase consisted of 60.0% acetonitrile and 40.0% ultrapure water, both containing 0.1% trifluoroacetic acid. Detection was carried out at an excitation wavelength of 236 nm and an emission wavelength of 310 nm. The flow rate was set at 1.0 mL/min, and the injection volume was 50.0 μL. If EE2 degradation follows pseudo-first-order kinetics, the apparent rate constants (k_{obs}) can be calculated from the slope of the linear regression of the natural logarithm of the concentration ratio at time t to the initial concentration ($\ln(C/C_0)$) versus irradiation time, as shown below (Eq. (S1)):

$$\ln\left(C/C_0\right) = -k_{obs}t \quad \text{(S1)}$$

here, C (mg/L) represents the concentration of EE2 at time *t* (min), C_0 (mg/L) is the initial concentration of EE2 (1.0 mg/L), and k_{obs} is the apparent rate constant for EE2 degradation, expressed in min^{-1}.

EPR Measurements

An agent 4-hydroxy-2,2,6,6-tetramethylpiperidine (TEMP, 200.0 μmol/L) was applied to trap $^1O_2$ in the EOM solution. The 5,5-dimethyl-1-pyrroline N-oxide (DMPO, 100.0 mmol/L) was used to examine $O_2^{\bullet-}$ and •OH in water and dimethyl

sulfoxide as the respective solvents. Specifically, 5.0 mgC/L EOM was mixed with 200.0 μmol/L freshly prepared TEMP in water, to trap $^1O_2$. The EOM also individually mixed with 100.0 mmol/L freshly prepared DMPO in water and dimethyl sulfoxide, to trap $O_2^{\bullet-}$ and •OH, respectively. After 20 min irradiation, 20 μL of the solution was immediately transferred to capillary tube and sealed at one end by vacuum grease. The capillary was fastened in the resonator. The signals of TEMP and $^1O_2$ adduct (TEMPO), DMPO and $O_2^{\bullet-}$ adduct (DMPO-OOH) or DMPO and •OH adduct (DMPO-OH) were detected using a Bruker A300 electron paramagnetic resonance (EPR) spectrometer, Germany. Measurement conditions were set as: a microwave power of 22.23 mW, sweep time of 40.0 s, a microwave frequency of 9.86 GHz, a modulation frequency of 100.0 kHz, a center magnetic field of 3520.0 G and a sweep width of 100.0 G for radicals, a center magnetic field of 3400.0 G and a sweep width of 1000.0 G for Mn(II).

Steady-state Concentrations of $^3EOM^*$ and $^1O_2$

The concentrations of residual TMP and FFA were quantified using HPLC equipped with an ultraviolet detector. For TMP analysis, the mobile phase consisted of 30.0% ultrapure water with 0.1% formic acid and 70.0% chromatographic-grade methanol, with detection at 220 nm and a retention time of 3.7 minutes. For FFA analysis, the mobile phase was composed of 15.0% ultrapure water containing 0.1% formic acid and 85.0% chromatographic-grade acetonitrile, with detection at 218 nm

and a retention time of 3.4 minutes. The flow rate was maintained at 1 mL/min, and the injection volume was set to 50 μL.

The steady-state concentration of triplet state EOM ($[^3EOM^*]_{SS}$) was calculated by dividing the degradation rate of TMP by the corresponding reaction rate constant, as described in Eq. (S2).

$$\left[^3EOM^*\right]_{SS} = \frac{d[TMP]}{-k_{TMP,^3EOM^*}[TMP]dt} + \frac{k_{TMP}}{-k_{TMP,^3EOM^*}} \quad (S2)$$

where the $k_{TMP,^3EOM^*}$ represents the rate constant of the bimolecular reaction between TMP and $^3EOM^*$ (8.1×10^8 $(mol/L)^{-1} \cdot s^{-1}$) (Erickson et al., 2018), [TMP] is the concentration of TMP (M), and k_{TMP} is the photodegradation rate constant of TMP in ultrapure water. The $[^3EOM^*]_{SS}$ can be obtained from Fig. S2a as 1.852×10^{-13} mol/L.

The steady-state concentration of singlet oxygen ($[^1O_2]_{SS}$) was calculated by dividing the degradation rate of FFA by its reaction rate constant with singlet oxygen, using Eq. (S3).

$$\left[^1O_2\right]_{SS} = \frac{d[FFA]}{-k_{FFA,^1O_2}[FFA]dt} + \frac{k_{FFA}}{-k_{FFA,^1O_2}} \quad (S3)$$

where the $k_{FFA,^1O2}$ represents the rate constant of the bimolecular reaction between FFA and $^1O_2$ (8.3×10^7 $(mol/L)^{-1} \cdot s^{-1}$) (Zeng et al., 2021), [FFA] is the concentration of FFA (mol/L), and k_{FFA} is the photodegradation rate constant of FFA in ultrapure water. The $[^1O_2]_{SS}$ can be obtained from Fig. S2b as 2.410×10^{-13} mol/L.

Steady-state Concentration of •OH

The concentration of 2-hydroxyterephthalic acid (2-hTPA) was quantified using

three-dimensional excitation-emission matrix (3D-EEM), with a bandpass slit width of 5 nm and a scanning speed of 2400 nm/min, at an excitation wavelength of 315 nm and an emission wavelength of 425 nm.

To determine the steady-state concentration of hydroxyl radicals ($[\bullet OH]_{SS}$), a range of TPA concentrations was employed to capture •OH, thereby generating 2-hTPA. The initial 2-hTPA formation rate ($R_{2\text{-hTPA}}$) is mathematically represented by Eq. (S4).

$$R_{2\text{-hTPA}} = \frac{d[2\text{-hTPA}]}{dt} = \eta k_{TPA,\bullet OH}[TPA][\bullet OH]_{SS} \quad (S4)$$

where η is the reaction yield, which is 35% according to the reference (Page et al., 2010). $k_{TPA,\bullet OH}$ represents the bimolecular reaction rate constant for the interaction between TPA and •OH, valued at 4.4×10^9 $(mol/L)^{-1} \cdot s^{-1}$ (Page et al., 2010). Additionally, the $[\bullet OH]_{SS}$ can also be expressed as Eq. (S5).

$$[\bullet OH]_{SS} = \frac{R_{\bullet OH}}{S + k_{TPA,\bullet OH}[TPA]} \quad (S5)$$

here, $R_{\bullet OH}$ represents the formation rate of •OH, and S is •OH scavenging rate constant by EOM. In the absence of TPA, Eq. (S5) can be simplified to $[\bullet OH]_{SS} = \frac{R_{\bullet OH}}{S}$.

By combining Eqs. (S4) and (S5), Eq. (S6) is derived.

$$R_{2\text{-hTPA}} = \eta k_{TPA,\bullet OH}[TPA] \frac{R_{\bullet OH}}{S + k_{TPA,\bullet OH}[TPA]} \quad (S6)$$

The variation of $R_{2\text{-hTPA}}$ as a function of [TPA] is depicted in Fig. S2d. When [TPA] approaches zero, Eq. (S6) becomes $R_{2\text{-hTPA}} = \eta k_{TPA,\bullet OH}[TPA] \frac{R_{\bullet OH}}{S}$. The slope of the tangent to the curve at this point is $\eta k_{TPA,\bullet OH} \frac{R_{\bullet OH}}{S}$. Therefore the $[\bullet OH]_{SS}$ generated

from EOM is calculated to be 2.392×10^{-13} mol/L.

Steady-state Concentration of $O_2^{\bullet-}$

The $O_2^{\bullet-}$ generated from irradiated EOM was measured using a flow injection analysis system (FIA, Waterville Analytical, USA), with the assistance of Professor Song Weihua and his colleagues. 2-methyl-6-[p-methoxyphenyl]-3,7-dihydroimidazo-[1,2-a]-pyrazin-3-one (MCLA), a methyl cypridina luciferin analogue, obtained from Tokyo Chemical Industry Co., Ltd. (Japan), was employed as a chemiluminescent reagent to quantify $O_2^{\bullet-}$ concentrations, following an established method (Li et al., 2023; Ma et al., 2020; Rose et al., 2008). Briefly, a 2.0 μmol/L MCLA solution was prepared in a 50.0 mmol/L sodium acetate buffer containing 1.0 μmol/L DTPA, with the pH adjusted to 6.0 using HCl. MCLA exhibits minimal reactivity with dissolved oxygen in solution and provides a linear response to $O_2^{\bullet-}$ concentrations up to 100.0 nmol/L (Fujimori et al., 1993). For $O_2^{\bullet-}$ measurement, the MCLA reagent and samples were continuously pumped at a maximum flow rate of 6.0 mL/min using a peristaltic pump. The solutions were then mixed in a 300 μL spiral glass flow cell, positioned beneath a photon counter (PMT, Hamamatsu HC135-11, Hamamatsu, Japan). When measuring $O_2^{\bullet-}$ concentrations in the nanomolar range, the PMT voltage was set to 880 V to optimize the signal-to-noise ratio. Additionally, MCLA produces background signals due to the auto-oxidation of its conjugate base with molecular oxygen or interactions with certain surfactants in the dark. The baseline values ranged from 300

to 600 counts in deionized water and typically from 6000 to 12,000 counts in the presence of dissolved organic matter. To accurately determine $O_2^{\bullet-}$ concentrations, baseline correction was applied. The baseline signals (S_b) were subtracted from the observed signal (S). The corrected signal counts were then converted into $O_2^{\bullet-}$ concentration using the following equation (Eq. (S7)).

$$[O_2^{\bullet-}] = \frac{(S\text{-}S_b)}{R} \tag{S7}$$

where R represents the slope obtained from the linear fitting of the calibration experiment, which is 1238.8 count/(nmol/L).

The transport time for samples from the beaker to the flow cell, where they are detected by the PMT, was approximately 16.0 seconds (residence time). The actual steady-state concentration of $O_2^{\bullet-}$ ($[O_2^{\bullet-}]_{SS}$) must be adjusted by shifting the measurement back by 16 seconds, referencing the response at time zero. The attenuation of $O_2^{\bullet-}$ during the residence time in the FIA pipeline can be described by Eq. (S8).

$$-\frac{d[O_2^{\bullet-}]}{dt} = 2k_d[O_2^{\bullet-}]^2 + k_{pseudo}[O_2^{\bullet-}] \tag{S8}$$

Rearranging and integrating Eq. (S8) yields Eq. (S9).

$$[O_2^{\bullet-}] = \frac{k_{pesudo}}{\left(\frac{k_{pesudo}}{[O_2^{\bullet-}]_{SS}} + 2k_d\right)e^{k_{pesudo}t} - 2k_d} \tag{S9}$$

here, k_{pesudo} represents the pseudo-first-order loss rate constant of $O_2^{\bullet-}$, while k_d is the second-order uncatalyzed dismutation rate constant of $O_2^{\bullet-}$, calculated as $(5.0 \times 10^{12}) \times [H^+]$ $(mol/L)^{-1} \cdot s^{-1}$ based on previous study (Rose et al., 2008). The fitting results are shown in Fig. S2f.

Electrochemical Measurements

The electrochemical measurements were conducted using a CHI760 electrochemistry workstation (Chenhua Co. Ltd., China), following the methodologies outlined in a previous study (Wang et al., 2023). Briefly, an Ag/AgCl electrode served as the reference electrode, a platinum mesh was used as the counter electrode, and a glassy carbon electrode with an area of 0.22 mm^2 was used as the working electrode. Cyclic voltammetry (CV) was performed in an electrolyte composed of 50.0 mmol/L Na_2SO_4, 1.0 mmol/L Mn(II), and 20.0 mg C/L EOM or 5.0 mmol/L PP, over a potential range of –0.4 to 1.2 V with a scanning rate of 50.0 mV/s. The CV parameters were as follows: initial scan polarity was negative, the number of sweep segments was 10, and the sample interval was 0.001 V.

Total Dissolved Mn and Mn(III) Determinations

At specified intervals during the experiments, 1.0 mL samples of the reaction solutions were collected in brown vials. The samples were immediately centrifuged at 12000 r/min for 10 minutes using an Allegra 64R centrifuge, and the concentrations of Mn(III) and total dissolved Mn (TD Mn) in the supernatant were subsequently measured. PP, a strong ligand that preferentially complexes with Mn(III), forms a stable Mn(III)-PP complex (log k_{app} = 31.35, pH = 8.0) which exhibits a distinct absorption peak at 258 nm in the UV-visible spectrum (ε = 6750 $(mol/L)^{-1}$) (Webb et

al., 2005). For quantification, a UV-2600 spectrophotometer (Shimadzu, Japan) was used. Following the determination of Mn(III), TD Mn was quantified using flame atomic absorption spectrometry (Z-2000, Hitachi, Japan). To reduce errors in measuring TD Mn and Mn(III), a Mn(III)-PP standard solution was employed. This solution was prepared by dissolving manganese(III) acetate dihydrate in an excess PP solution at pH 8.0, resulting in a clear pink solution, following a previously established method (Madison et al., 2011).

Text S3 Products preparation and analysis of EE2.

Products Extraction

The enrichment and separation of samples were conducted via solid-phase extraction (SPE). Before extraction, the SPE column (Bond Elut-PPL, Agilent, USA) was sequentially conditioned with 10.0 mL of ethyl acetate, 30.0 mL of methanol, and 15.0 mL of ultrapure water at a flow rate of 1.0 mL/min. The solutions after different reaction times were then passed through the SPE column at the same flow rate. The column was rinsed with 5.0 mL of ultrapure water/methanol (9:1, *v*/*v*) and dried under vacuum. The target compounds were eluted with 15.0 mL of ethyl acetate at 1.0 mL/min. The eluent was collected and transferred to a liquid chromatography vial for further analysis.

LC-Q-TOF-MS Instrumental Parameters

A liquid chromatograph quadrupole-time of flight-mass spectrometer (LC-Q-TOF-MS), equipped with a C18 column (waters BEH C18, 2.1 × 100 mm, 1.7 μm), was used to analyze the degradation products of EE2. The mobile phases consisted of acetonitrile (A) and 0.1% formic acid (B), with the following gradient elution conditions: 0 minutes: 8% A, 92% B; 2.5 minutes: 35% A, 65% B; 5 minutes: 80% A, 20% B; 6.5 minutes: 98% A, 2% B; 11 minutes: 98% A, 2% B; 11.2 minutes: 8% A, 92% B; 14 minutes: 8% A, 92% B. The flow rate was set at 0.3 mL/min, with an injection volume of 5 μL, and the column temperature was maintained at 40 °C. In the

mass spectrometer, positive ion full scan mode was employed, with a scanning range of 50 to 1000 m/z. The electrospray ionization source operated at 4000 V, with an atomization air flow of 3.0 L/min, a drying air flow rate of 10.0 L/min, a total flow rate of 10.0 L/min, a heating module temperature of 400 °C, a pipe temperature of 250 °C, and an interface temperature of 300 °C.

Text S4 Quantification of the relative contribution of Mn(III), MnO_x, and EOM to EE2 degradation.

Initial Observations

In this experiment, EE2 photodegradation in the presence of EOM, MnO_x, and their combination was found to follow pseudo-first-order kinetics under all conditions. Self-photodegradation of EE2 was found to be changed minor in the current study as 5.56×10^{-4} min^{-1}. Additionally, EOM can reduce MnO_x via $O_2^{\bullet-}$ reduction, which results in the formation of Mn(III), an active intermediate that further accelerates EE2 degradation.

Synergistic Effect and Its Attribution

The presence of both EOM and MnO_x increases the photodegradation rate of EE2 more than when either is present individually. The combined degradation rate constant does not match the sum of the individual degradation rates. This indicates a synergistic effect. The synergistic contribution can be calculated as Eq. (S10).

$$k_{synergy} = k_{EOM+MnO_x} - k_{EOM} - k_{MnO_x} - k_{EE2} \quad (S10)$$

where $k_{synergy}$ represents the additional degradation rate due to the interaction between EOM and MnO_x beyond their individual contributions (min^{-1}), $k_{EOM+MnOx}$ is the combined EE2 photodegradation rate constant, k_{EOM} and k_{MnOx} are EOM and MnO_x mediated EE2 photodegradation rate constant, respectively, k_{EE2} is self-photodegradation of EE2, as 5.56×10^{-4} min^{-1}.

The percentage contribution of the synergy can be calculated as Eq. (S11).

$$\text{Synergistic Contribution} = \frac{k_{\text{synergy}}}{k_{\text{EOM+MnO}_x}} \times 100\% \quad \text{(S11)}$$

Distribution of Synergistic Contribution

EOM primarily accelerates EE2 degradation by generating reactive species such as $^3\text{EOM}^*$, $^1\text{O}_2$, and •OH, while MnO_x acts directly as an oxidant in this process. Additionally, $\text{O}_2^{\bullet-}$ produced by EOM influence the reduction of MnO_x, leading to the formation of the reactive intermediate Mn(III), which contributes to further EE2 degradation. Importantly, the primary reactive species influencing EE2 do not engage in MnO_x reductive dissolution. Given that the contributions of EOM and MnO_x to the reaction are not identical, it is reasonable to assume that the synergistic effect primarily arises from their interaction, with Mn(III) formation being one of its outcomes. Consequently, the synergistic effect should be allocated based on the respective reaction rate constants of EOM and MnO_x. We assume that components with larger rate constants will capture a greater share of the synergistic effect. The fraction of synergy attributed to each component and its contribution can be calculated using Eqs. (S12) and (S13).

$$\text{EOM Synergy Fraction} = \frac{k_{\text{EOM}}}{k_{\text{EOM}} + k_{\text{MnO}_x}} \times \text{Synergistic Contribution} \quad \text{(S12)}$$

$$\text{MnO}_x\text{ Synergy Fraction} = \frac{k_{\text{MnO}_x}}{k_{\text{EOM}} + k_{\text{MnO}_x}} \times \text{Synergistic Contribution} \quad \text{(S13)}$$

Final Contribution Calculation

We now calculate the total contribution of each component by adding the synergistic contributions to the individual contributions by Eqs. (S14), (S15) and (S16).

$$Toatl_{\mathrm{EOM}} = \frac{k_{\mathrm{EOM}}}{k_{\mathrm{EOM+MnO}_x}} \times 100\% + \text{EOM Synergy Fraction} \quad \text{(S14)}$$

$$Toatl_{\mathrm{MnO}_x} = \frac{k_{\mathrm{MnO}_x}}{k_{\mathrm{EOM+MnO}_x}} \times 100\% + \mathrm{MnO}_x \text{ Synergy Fraction} \quad \text{(S15)}$$

$$Toatl_{\mathrm{Mn(III)}} = \left. \frac{R_{\mathrm{O_2^{\bullet-}-MnO}_x}}{[\mathrm{EE2}]} \right/ k_{\mathrm{EOM+MnO}_x} \times 100\%$$

$$= \left. \frac{k_{\mathrm{O_2^{\bullet-}-MnO}_x} \times [\mathrm{O_2^{\bullet-}}]_{\mathrm{SS}} \times [\mathrm{MnO}_x]}{[\mathrm{EE2}]} \right/ k_{\mathrm{EOM+MnO}_x} \times 100\% \quad \text{(S16)}$$

where $R_{\mathrm{O_2^{\bullet-}-MnO}_x}$ is the apparent second-order rate constant for MnO_x reductive dissolution by $O_2^{\bullet-}$ ($(\mu mol/L)^{-1} \cdot min^{-1}$), $[O_2^{\bullet-}]_{SS}$ is the steady-state concentration of $O_2^{\bullet-}$ (nmol/L), $[MnO_x]$ is MnO_x concentration (100.0 μmol/L), and [EE2] is EE2 concentration (1.0 mg/L).

We then divide each contribution by the total and scale them down to normalized their contributions using Eq. (S17).

$$C_{\mathrm{A}} = \frac{Toatl_{\mathrm{A}}}{Toatl_{\mathrm{EOM}} + Toatl_{\mathrm{MnO}_x} + Toatl_{\mathrm{Mn(III)}}} \quad \text{(S17)}$$

where C_A represents the contribution of each component on EE2 photodegradation, $Total_A$ is the total contribution of each component by adding the synergistic contributions to the individual contributions.

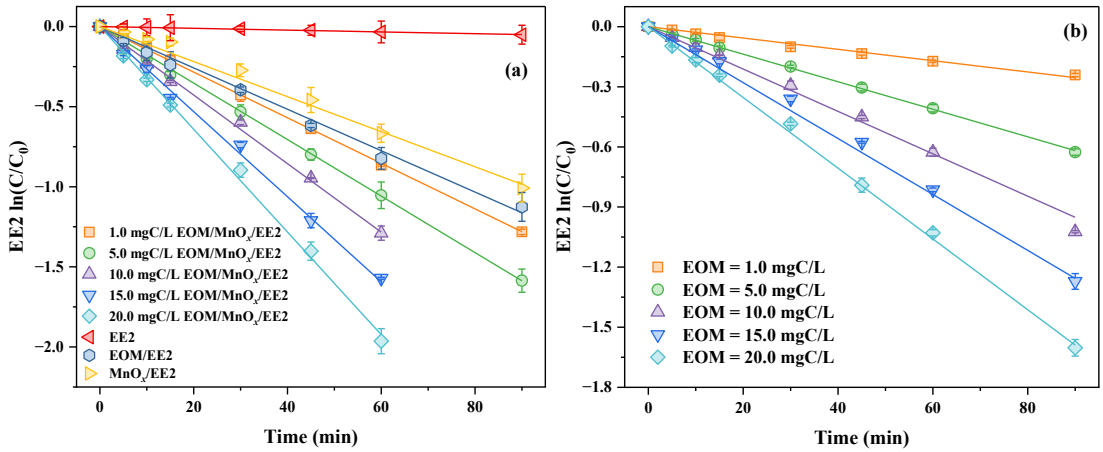

Fig. S1. Photodegradation kinetics of EE2 at different EOM concentrations (a) in the presence or (b) in the absence of MnO_x. Experimental conditions: [MnO_x] = 100.0 μmol/L, [EE2] = 1.0 mg/L, [pH] = 8.0.

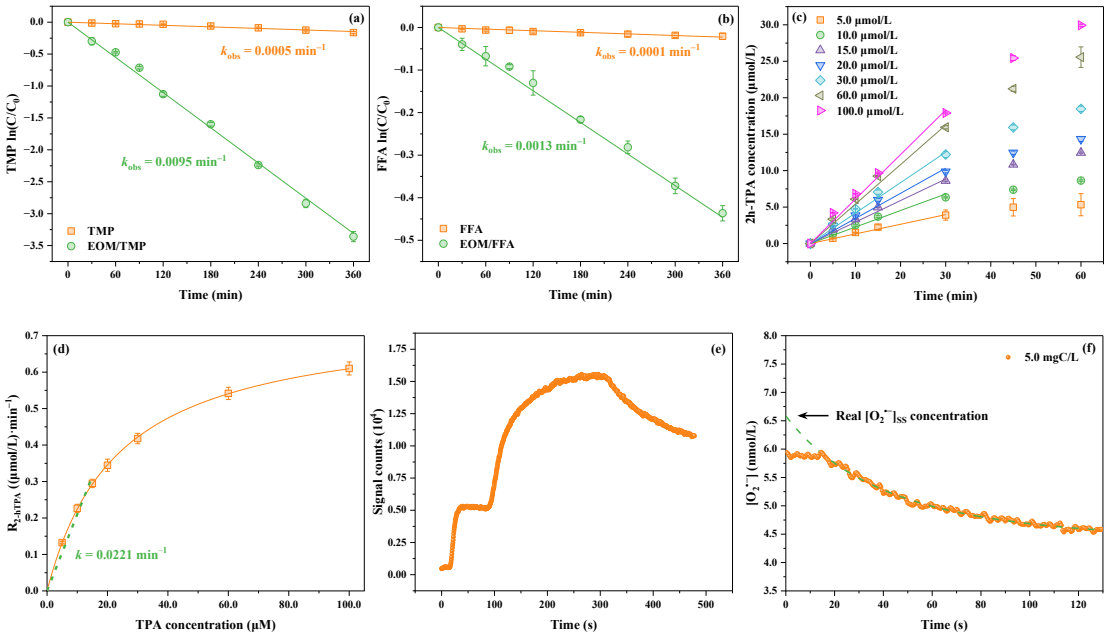

Fig. S2. The removal of (a) TMP and (b) FFA in EOM solution. (c) Concentration and (d) formation rate of 2h-TPA from varied concentrations of TPA in EOM solutions under irradiation. (e) Chemiluminescent signal counts generated from irradiated EOM solutions. (f) Measured $O_2^{\bullet-}$ (nmol/L) during irradiations and decay experiments (dots) and $O_2^{\bullet-}$ decay fitted as Eqs. (S8) and (S9) (green dot line). The actual steady-state concentration of $O_2^{\bullet-}$ can be derived from the fitted curve by referencing the response at time zero. Experimental conditions: [EOM] = 5.0 mgC/L, [TMP] = 100.0 μmol/L, [FFA] = 50.0 μmol/L, [TPA] = 5.0–100.0 μmol/L, [pH] = 8.0.

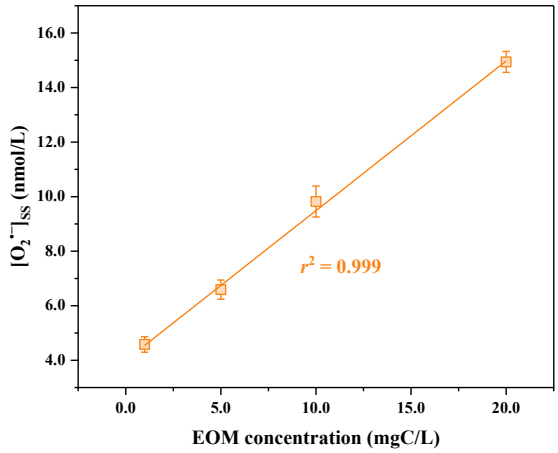

Fig. S3. Steady-state concentrations of $O_2^{\bullet-}$ at different EOM concentrations. Experimental conditions: [pH] = 8.0.

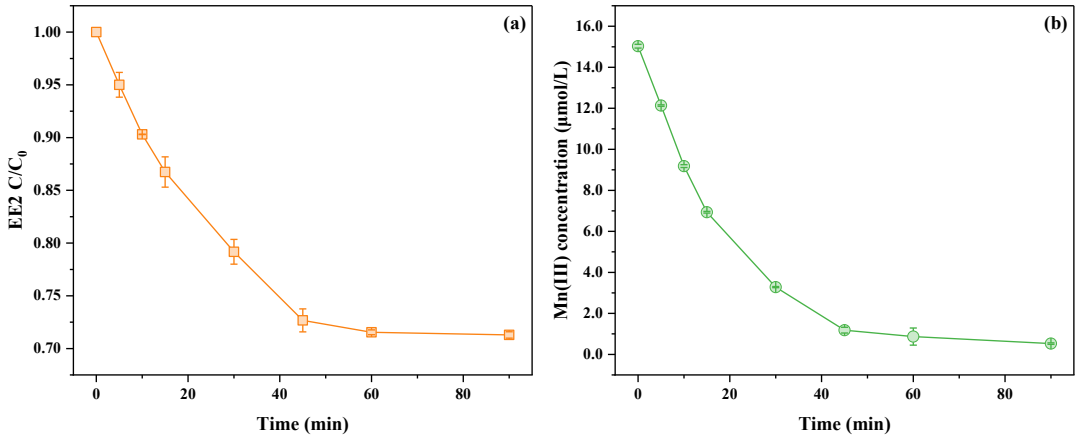

Fig. S4. (a) EE2 removal by supernatant of the EOM and MnO_x mixture after the reaction and (b) the change of Mn(III) during the reaction. Experimental conditions: [Mn(III)] = 15.0 μmol/L, [EE2] = 1.0 mg/L, [pH] = 8.0.

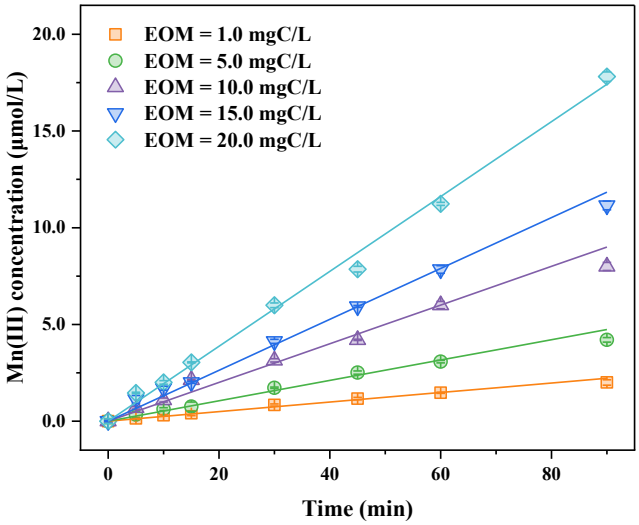

Fig. S5. Photogeneration kinetics of Mn(III) at different EOM concentrations. Experimental conditions: [MnO_x] = 100.0 μmol/L, [PP] = 5.0 mmol/L, [pH] = 8.0.

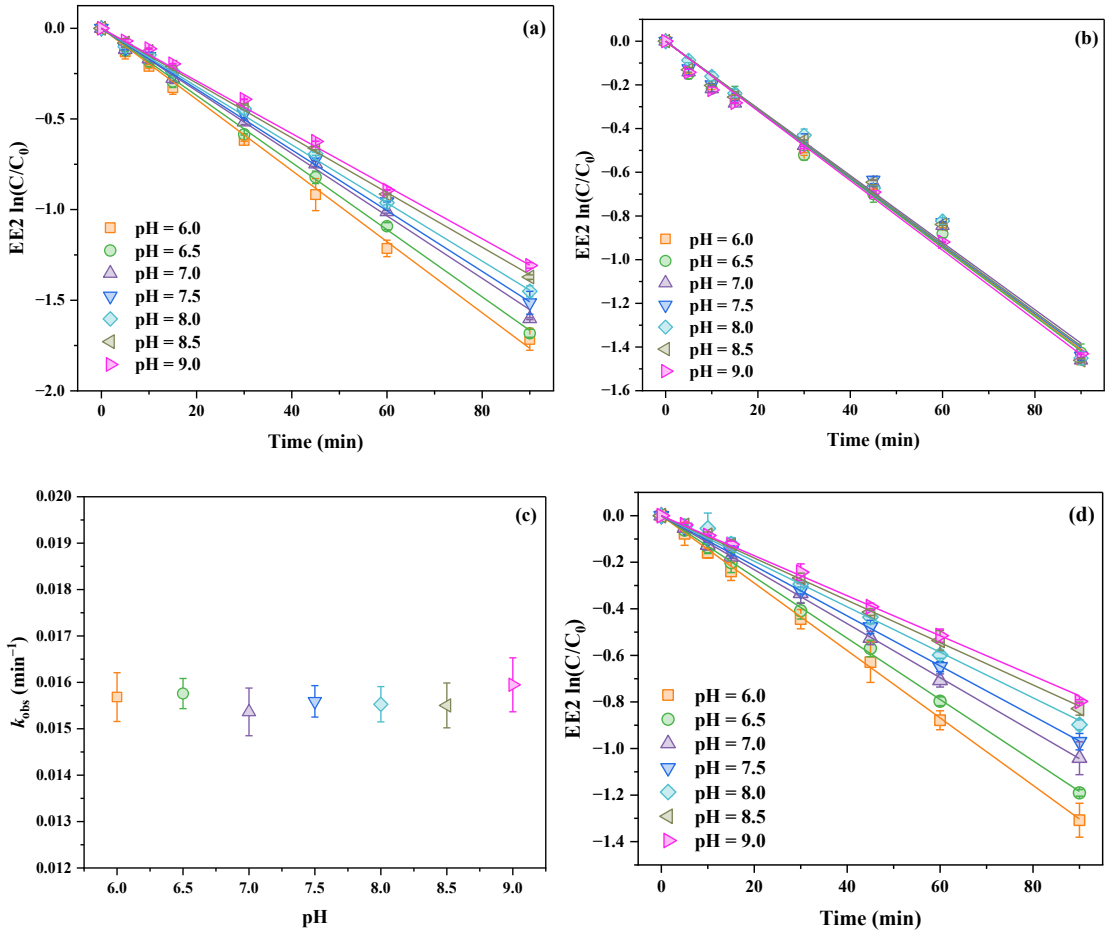

Fig. S6. Photodegradation kinetics of EE2 at different pH conditions in (a) EOM and MnO_x mixture, (b) in EOM solution and (d) in MnO_x solution. (c) The apparent degradation rate constants of EE2 in EOM solution. Experimental conditions: [EOM] = 5.0 mgC/L, [MnO_x] = 100.0 μmol/L, [EE2] = 1.0 mg/L.

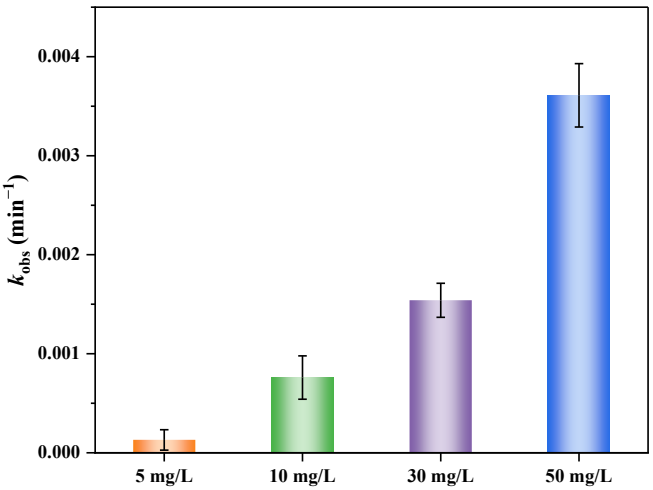

Fig. S7. Observed EE2 photodegradation rates at various NO_3^- concentrations. Experimental conditions: [EE2] = 1.0 mg/L, [pH] = 8.0.

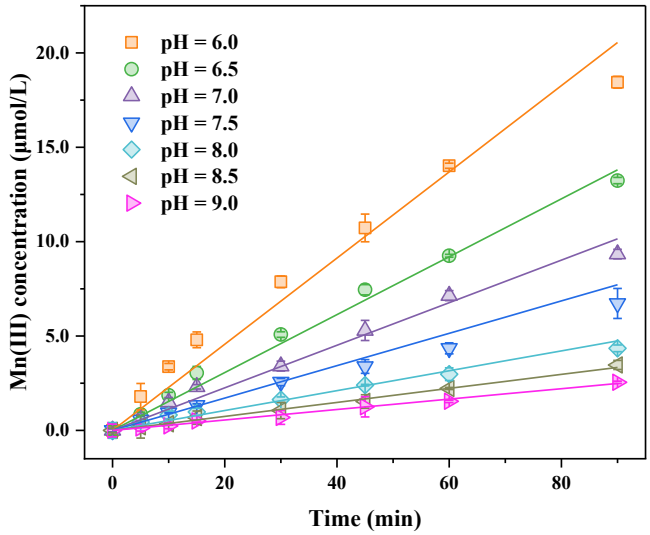

Fig. S8. Photogeneration kinetics of Mn(III) at different pH conditions. Experimental conditions:

[EOM] = 5.0 mgC/L, [MnO_x] = 100.0 μmol/L, [PP] = 5.0 mmol/L.

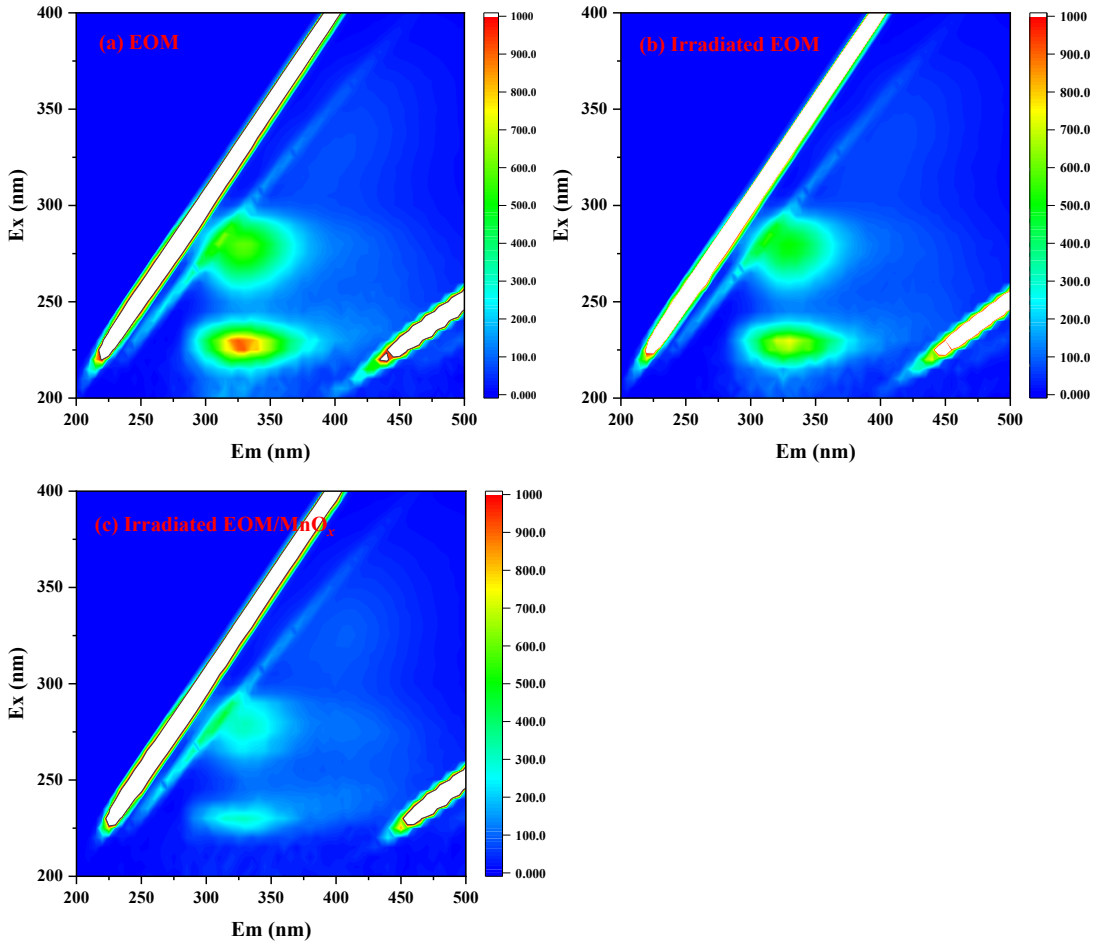

Fig. S9. The EEM spectra of (a) the initial EOM, irradiated EOM, and irradiated EOM in the presence of MnO_x.

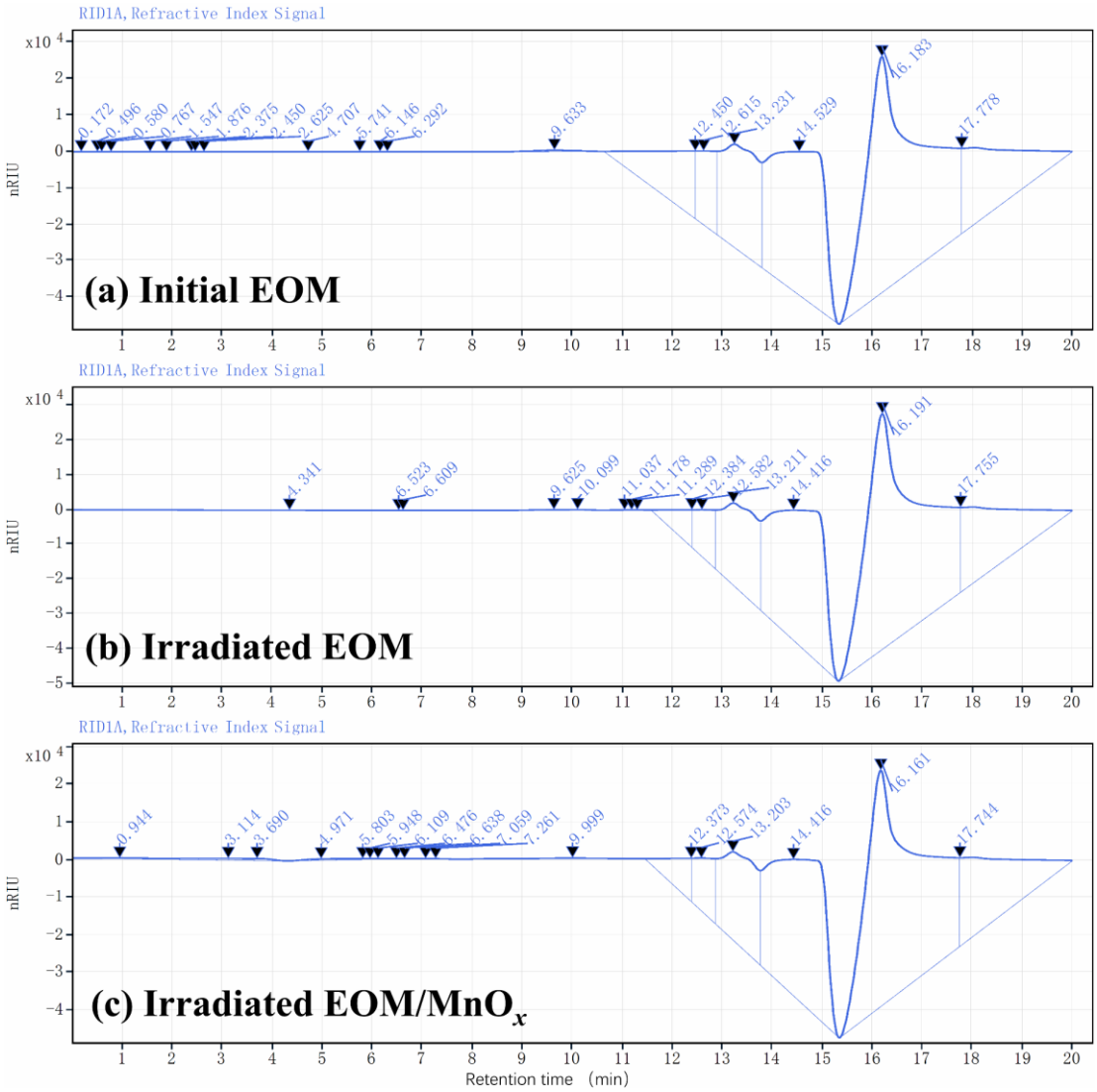

Fig. S10. The molecular weight distribution of (a) initial EOM, (b) irradiated EOM, and (c) irradiated EOM in the presence of MnO_x by high-performance size-exclusion chromatography with refractive index detection.

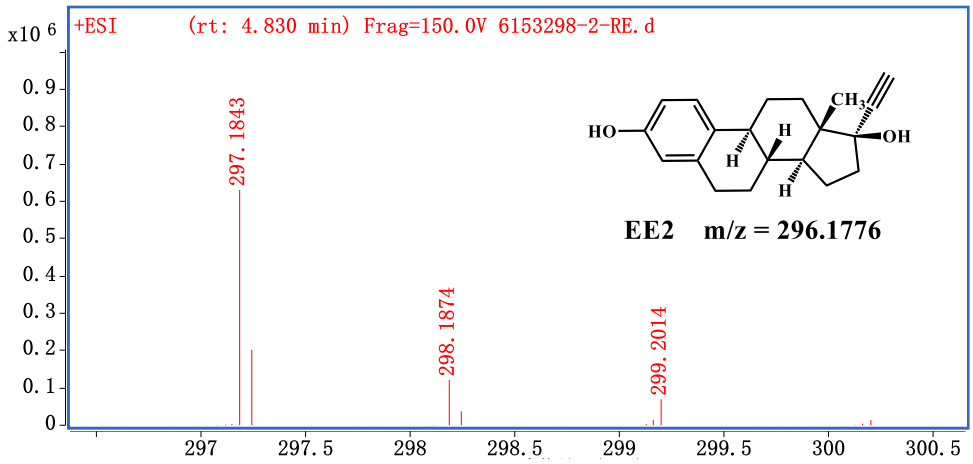
x10 6
+ESI (rt: 4.830 min) Frag=150.0V 6153298-2-RE.d
297.1843
298.1874
299.2014
EE2 m/z = 296.1776

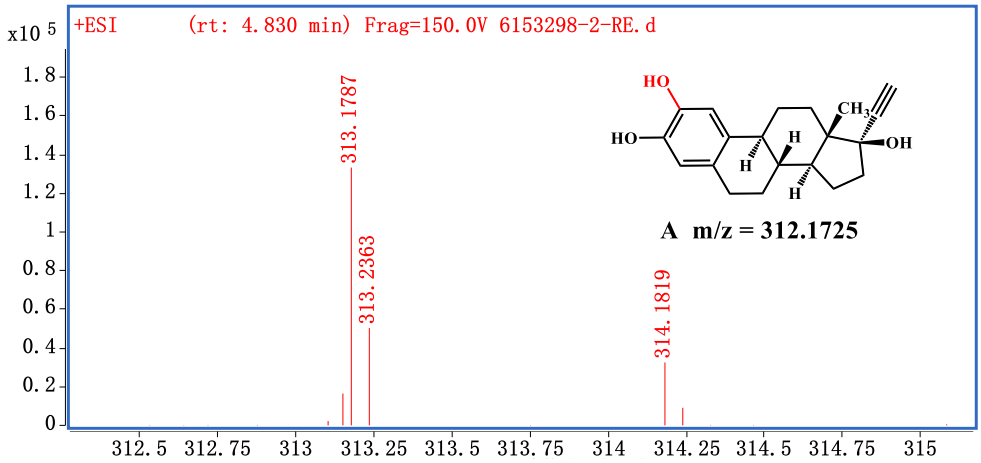
x10 5
+ESI (rt: 4.830 min) Frag=150.0V 6153298-2-RE.d
313.1787
313.2363
314.1819
A m/z = 312.1725

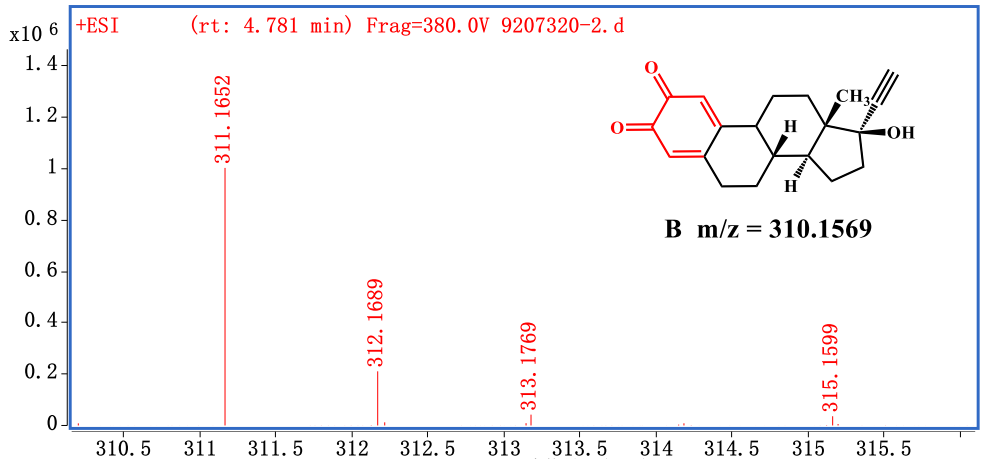
x10 6
+ESI (rt: 4.781 min) Frag=380.0V 9207320-2.d
311.1652
312.1689
313.1769
315.1599
B m/z = 310.1569

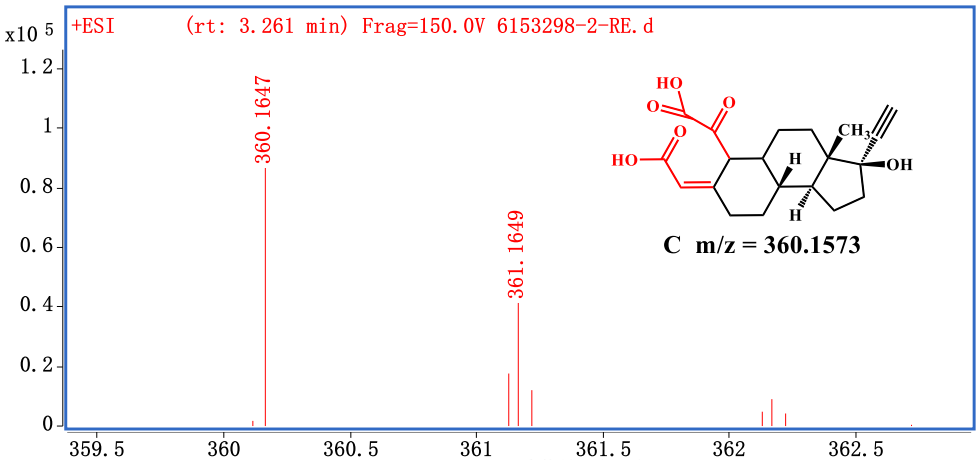
x10 5
+ESI (rt: 3.261 min) Frag=150.0V 6153298-2-RE.d
360.1647
361.1649
HO
O
O
O
HO
CH3
H
H
OH
C m/z = 360.1573

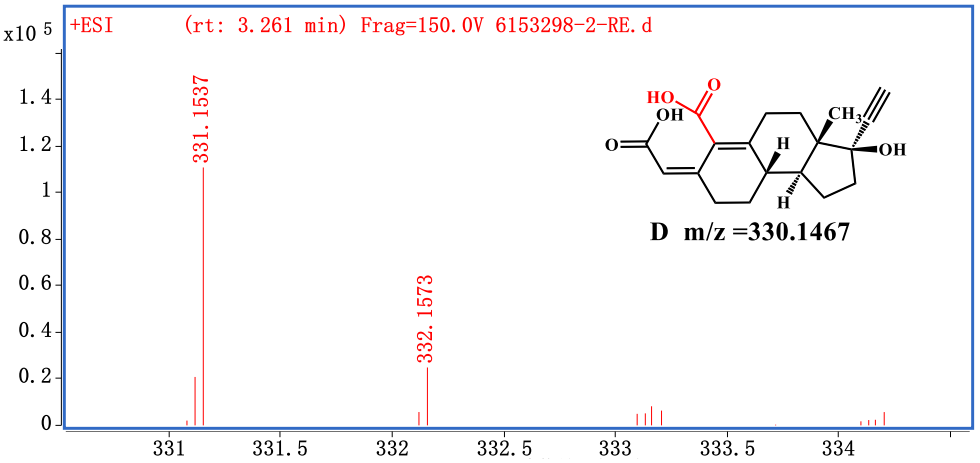
x10 5
+ESI (rt: 3.261 min) Frag=150.0V 6153298-2-RE.d
331.1537
332.1573
HO
OH
O
O
CH3
H
H
OH
D m/z =330.1467

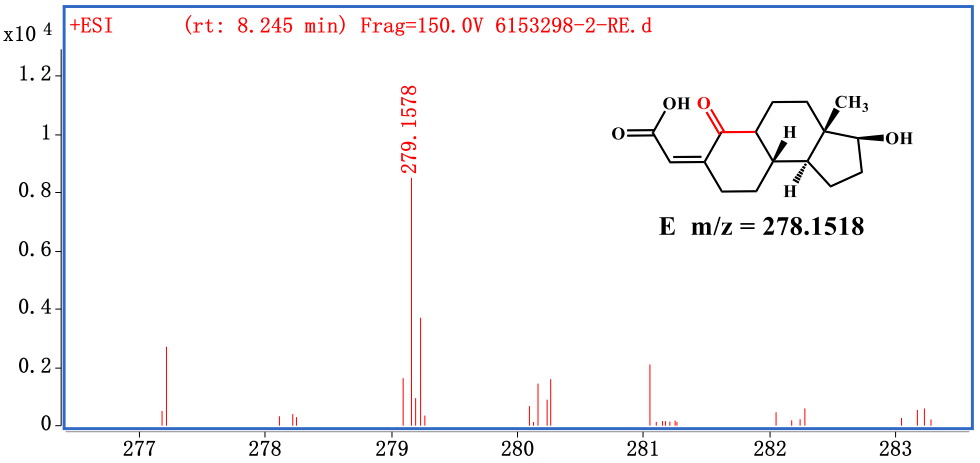
x10 4
+ESI (rt: 8.245 min) Frag=150.0V 6153298-2-RE.d
279.1578
OH
O
O
CH3
H
H
OH
E m/z = 278.1518

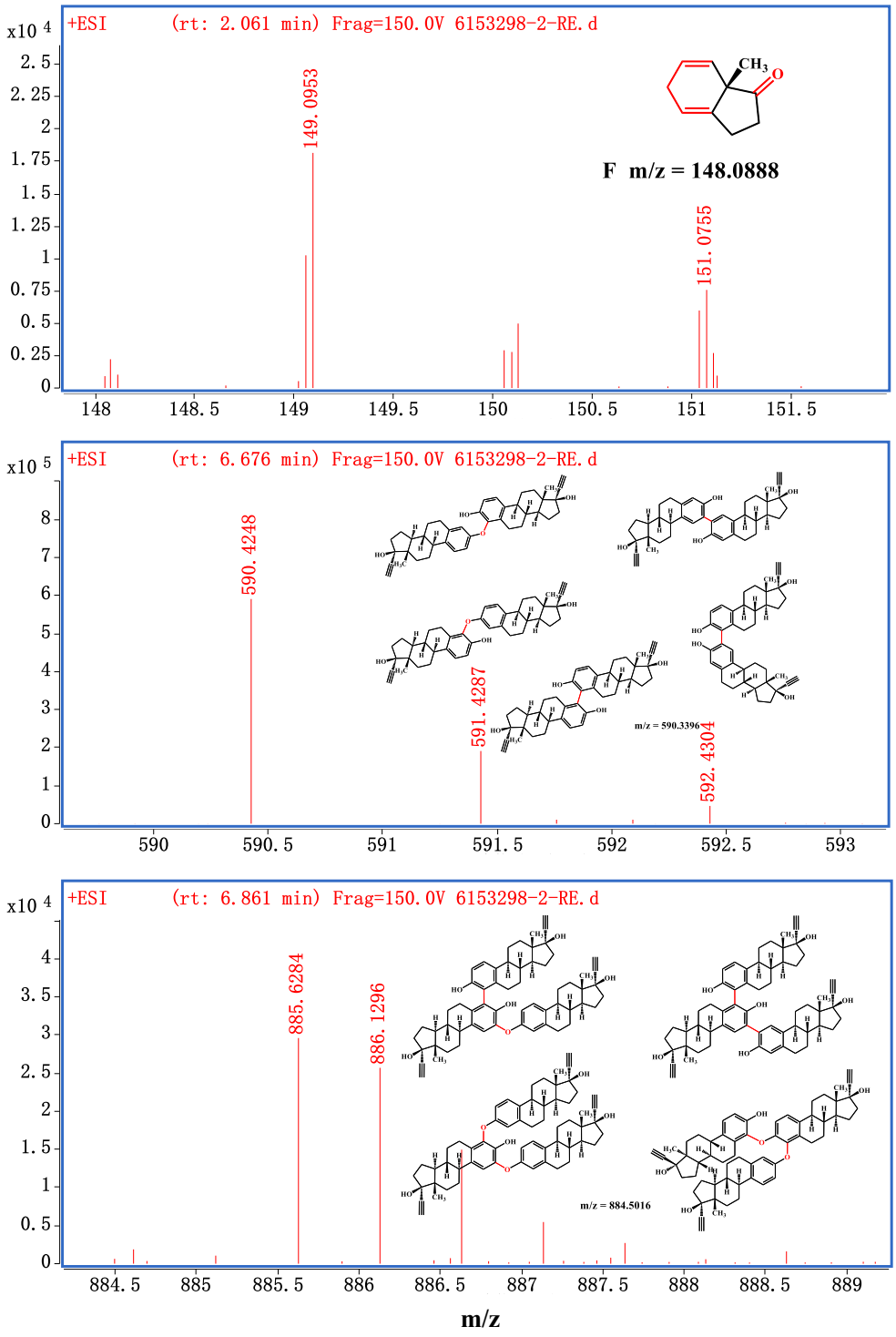

Fig. S11. The LC-Q-TOF-MS extracted ion current chromatograms of EE2 and different intermediates at different reaction times.

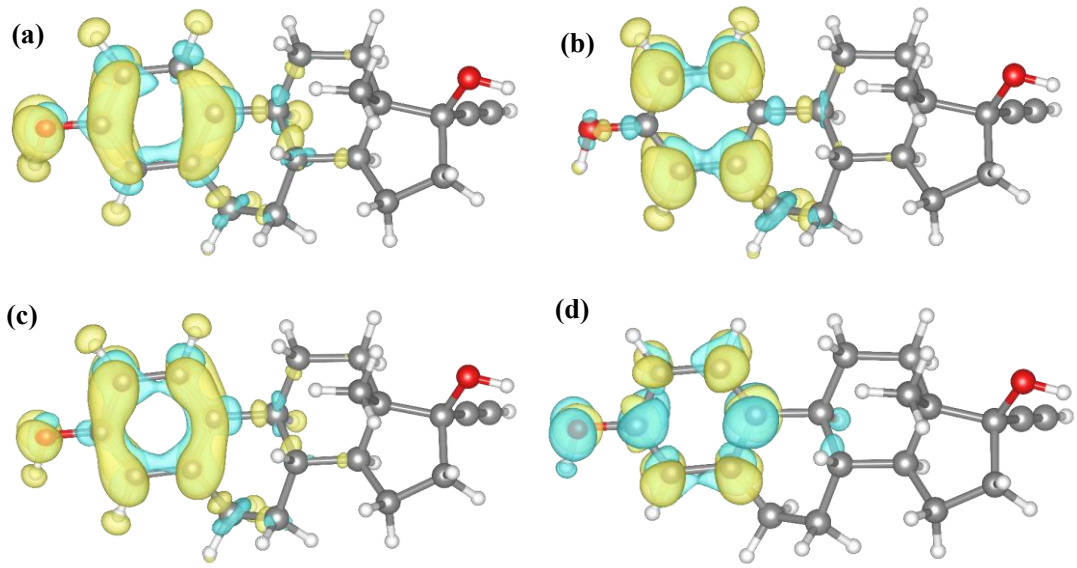

Fig. S12. (a) f^-, (b) f^+, (c) f^0, and (d) DD of EE2 with an isovalue of 0.003.

Table S1. Peak areas of initial, irradiated EOM, and irradiated EOM in the presence of MnO_x at different retention times.

Initial EOM		Irradiated EOM		Irradiated EOM with MnO_x	
Retention time (min)	Peak area	Retention time (min)	Peak area	Retention time (min)	Peak area
0.172	11.836	4.341	30.131	0.944	26440.090
0.496	14.138	6.523	14.055	3.114	14613.758
0.58	14.216	6.609	70.836	3.690	28656.407
0.767	16.334	9.625	7735.358	4.971	23352.944
1.547	21.789	10.099	5329.174	5.803	1549.377
1.876	22.583	11.037	752.167	5.948	2575.111
2.375	33.172	11.178	190.795	6.109	1876.227
2.450	26.83	11.289	234.913	6.476	117.631
2.625	27.403	12.384	266674.584	6.638	112.808
4.707	24.672	12.582	390510.831	7.059	596.005
5.741	18.471	13.211	1252648.228	7.261	1561.465
6.146	20.443	14.416	2970266.471	9.999	21415.416
6.292	14.038	–	–	12.373	324818.332
9.633	22178.175	–	–	12.574	418350.092
12.450	1021500.02	–	–	13.203	1232998.833
12.615	537627.223	–	–	14.416	2935109.640
13.231	1491953.989	–	–	16.161	4646903.015
14.529	3005160.511	–	–	17.744	1596832.033
16.183	4784656.221	–	–	–	–
17.778	1562058.765	–	–	–	–

Table S2. Fukui function index of EE2.

Atom	q(N)	q(N+1)	q(N-1)	f^-	f^+	f^0	CDD
1(C)	0.061	0.0079	0.1644	0.1034	0.0532	0.0783	-0.0502
2(C)	-0.0782	-0.1965	-0.015	0.0632	0.1183	0.0907	0.0551
3(C)	-0.0041	-0.1107	0.0584	0.0625	0.1065	0.0845	0.0441
4(C)	-0.0207	-0.0618	0.0916	0.1123	0.0411	0.0767	-0.0711
5(C)	-0.052	-0.1708	0.0068	0.0588	0.1188	0.0888	0.06
6(C)	-0.0783	-0.2081	0.0235	0.1018	0.1298	0.1158	0.0281
7(C)	-0.0463	-0.0698	-0.0322	0.0142	0.0235	0.0188	0.0093
8(C)	-0.0154	-0.0206	-0.0012	0.0142	0.0052	0.0097	-0.009
9(C)	-0.016	-0.0188	-0.0072	0.0088	0.0028	0.0058	-0.006
10(C)	-0.046	-0.0578	-0.0385	0.0076	0.0117	0.0096	0.0041
11(C)	-0.0215	-0.0235	-0.018	0.0035	0.002	0.0027	-0.0015
12(C)	0.0141	0.0138	0.014	0	0.0003	0.0001	0.0003
13(C)	-0.0541	-0.058	-0.0499	0.0042	0.0039	0.0041	-0.0002
14(C)	-0.0481	-0.0532	-0.0433	0.0047	0.0052	0.0049	0.0004
15(H)	0.036	0.0143	0.054	0.018	0.0217	0.0199	0.0037
16(H)	0.0448	-0.0071	0.0797	0.0349	0.0518	0.0434	0.0169
17(H)	0.0422	-0.0071	0.0739	0.0316	0.0493	0.0405	0.0177
18(H)	0.0434	-0.0134	0.087	0.0436	0.0568	0.0502	0.0132
19(H)	0.0298	0.0175	0.0405	0.0107	0.0122	0.0115	0.0015
20(H)	0.0276	0.0221	0.0345	0.0069	0.0055	0.0062	-0.0014
21(H)	0.0309	0.0226	0.0398	0.0089	0.0084	0.0086	-0.0005
22(C)	0.0989	0.098	0.1001	0.0011	0.001	0.001	-0.0001
23(C)	-0.0507	-0.0531	-0.0471	0.0037	0.0023	0.003	-0.0014
24(H)	0.0313	0.0281	0.0351	0.0037	0.0033	0.0035	-0.0004
25(C)	-0.0532	-0.0549	-0.0508	0.0025	0.0017	0.0021	-0.0008
26(H)	0.0335	0.0317	0.0359	0.0024	0.0018	0.0021	-0.0006

27(H)	0.0321	0.0301	0.0348	0.0027	0.002	0.0024	-0.0007
28(H)	0.03	0.0276	0.0334	0.0034	0.0024	0.0029	-0.001
29(H)	0.0347	-0.0018	0.056	0.0214	0.0365	0.0289	0.0151
30(H)	0.0295	0.0117	0.0409	0.0114	0.0178	0.0146	0.0065
31(H)	0.0215	0.0177	0.0257	0.0043	0.0038	0.004	-0.0004
32(H)	0.0268	0.0194	0.0343	0.0074	0.0074	0.0074	0
33(H)	0.0291	0.0159	0.0576	0.0286	0.0132	0.0209	-0.0154
34(H)	0.024	0.017	0.0336	0.0096	0.0071	0.0083	-0.0025
35(O)	-0.2124	-0.2467	-0.0895	0.1229	0.0343	0.0786	-0.0886
36(H)	0.1905	0.1707	0.2306	0.0401	0.0199	0.03	-0.0203
37(C)	-0.091	-0.092	-0.0898	0.0012	0.001	0.0011	-0.0002
38(H)	0.0302	0.0283	0.0325	0.0024	0.0019	0.0021	-0.0004
39(H)	0.0267	0.0244	0.0297	0.003	0.0023	0.0027	-0.0007
40(H)	0.0295	0.0285	0.0306	0.001	0.0011	0.0011	0
41(H)	0.0222	0.0185	0.0268	0.0046	0.0037	0.0041	-0.0009
42(O)	-0.232	-0.2336	-0.2301	0.0019	0.0015	0.0017	-0.0004
43(H)	0.1738	0.1724	0.1755	0.0017	0.0014	0.0016	-0.0003
44(C)	-0.0531	-0.0529	-0.0536	-0.0005	-0.0002	-0.0003	0.0003
45(C)	-0.1193	-0.123	-0.1148	0.0045	0.0037	0.0041	-0.0008
46(H)	0.0984	0.0971	0.0999	0.0015	0.0012	0.0014	-0.0003

References

Erickson, P. R., Moor, K. J., Werner, J. J., Latch, D. E., Arnold, W. A. and McNeill, K., 2018. Singlet oxygen phosphorescence as a probe for triplet-state dissolved organic matter reactivity. Environ. Sci. Technol. 52, 9170-9178.

Fujimori, K., Nakajima, H., Akutsu, K., Mitani, M., Sawada, H. and Nakayama, M., 1993. Chemiluminescence of cypridina luciferin analogues. part 1. effect of pH on rates of spontaneous autoxidation of CLA in aqueous buffer solutions. J. Chem. Soc. Perk. T. 2, 2405-2409.

Li, Q., Yan, S. W., Xiao, R. Y. and Song, W. H., 2023. Kinetic and mechanistic considerations of the photosensitized transformation of chlorine in chromophoric dissolved organic matter solutions under simulated solar irradiation. Environ. Sci. Technol. 57, 8446-8456.

Ma, J. Z., Nie, J. X., Zhou, H. X., Wang, H., Lian, L. S., Yan, S. W. and Song, W. H., 2020. Kinetic consideration of photochemical formation and decay of superoxide radical in dissolved organic matter solutions. Environ. Sci. Technol. 54, 3199-3208.

Madison, A. S., Tebo, B. M. and Luther, G. W., 2011. Simultaneous determination of soluble manganese(III), manganese(II) and total manganese in natural (pore) waters. Talanta 84, 374-381.

Page, S. E., Arnold, W. A. and McNeill, K., 2010. Terephthalate as a probe for photochemically generated hydroxyl radical. J. Environ. Monit. 12, 1658-1665.

Rose, A. L., Moffett, J. W. and Waite, T. D., 2008. Determination of superoxide in

seawater using 2-methyl-6-(4-methoxyphenyl)-3,7-dihydroimidazo 1,2-a pyrazin-3(7*H*)-one chemiluminescence. Anal. Chem. 80, 1215-1227.

Wang, J. Q., Chai, Z. Z., Yang, S., Du, E. D. and Guo, H. G., 2023. Insights into the electron transfer regime of permanganate activation on carbon nanomaterial reduced from carbon dioxide. J. Hazard. Mater. 459, 132094.

Webb, S. M., Dick, G. J., Bargar, J. R. and Tebo, B. M., 2005. Evidence for the presence of Mn(III) intermediates in the bacterial oxidation of Mn(II). Proc. Natl. Acad. Sci. U. S. A. 102, 5558-5563.

Zeng, Y., Fang, G., Fu, Q., Dionysiou, D. D., Wang, X., Gao, J., Zhou, D. and Wang, Y., 2021. Photochemical characterization of paddy water during rice cultivation: Formation of reactive intermediates for As(III) oxidation. Water Res. 206, 117721.